UNIVERSITY OF CALIFORNIA, SAN DIEGO

A Novel Multi-Scale Model of Time-Scale Integration for Modeling the Hemodynamics of the Cardiovascular System

A Thesis submitted in partial satisfaction of the requirements
for the degree Master of Science

in

Bioengineering

by

Jessica Caitlin Leon

Committee in charge:

Professor Andrew D. McCulloch, Chair
Professor Jeffery H. Omens, Co-Chair
Professor Pedro J. Cabrales Arevalo

2017

The Thesis of Jessica Caitlin Leon is approved, and it is acceptable in quality and form for publication on microfilm and electronically:

_____

_____

Co-Chair

_____

Chair

University of California, San Diego

2017

DEDICATION

In recognition of my family, in particular my parents, Diane Leon and Nathan Leon. Thank you for instilling in me the value of hard work and the belief that I can do anything I set my mind to. Thank you for enduring my seemingly endless questions as I was growing up, without quenching my thirst for knowledge. Thank you also for your unconditional love and support, which has contributed in no small part to getting me to where I am today.

EPIGRAPH

“Simplicity is the ultimate sophistication.” –Leonardo da Vinci

TABLE OF CONTENTS

LIST OF ABBREVIATIONS

3-D	Three-Dimensional
ADH	Anti-Diuretic Hormone
AS	Aortic Stenosis
AV	Atrioventricular
CO	Cardiac Output
CNS	Central Nervous System
EDPVR	End-Diastolic Pressure-Volume Relationship
ESPVR	End-Systolic Pressure-Volume Relationship
ESP	End-Systolic Pressure
FEM	Finite Element Method
GFR	Glomerular Filtration Rate
LA	Left Atrium
LV	Left Ventricle
LVP	Left Ventricular Pressure
MAP	Mean Arterial Pressure
ODE	Ordinary Differential Equation
PV	Pressure-Volume
RA	Right Atria
RAAS	Renin-Angiotensin-Aldosterone System
RV	Right Ventricle
SA	Sinoatrial
SVR	Systemic Vascular Resistance

LIST OF FIGURES

LIST OF TABLES

ACKNOWLEDGEMENTS

I would like to acknowledge Dr. Andrew McCulloch, Dr. Jeffery Omens, Dr. Amir Nikou, Dr. Daniel A. Beard, and Dr. Kyoko Yoshida for their guidance, support, and contributions to the development of this work.

ABSTRACT OF THE THESIS

A Novel Multi-Scale Model of Time-Scale Integration for Modeling the Hemodynamics of the Cardiovascular System

by

Jessica Caitlin Leon

Master of Science in Bioengineering

University of California, San Diego, 2017

Professor Andrew D. McCulloch, Chair
Professor Jeffery H. Omens, Co-Chair

The cardiovascular system is regulated through numerous control systems, which operate on various time scales. The baroreflex operates on the scale of seconds to minutes, responding to acute changes in pressure by altering heart rate, heart contractility, and blood vessel diameter. Blood volume control operates on a time scale of minutes to hours, in which the kidneys regulate blood pressure by means of blood plasma osmolarity and volume in the circulatory system. When pressure is altered on a

longer time scale of days to years, growth and remodeling occur in the heart and blood vessel walls.

In this thesis, a multi-scale model was created to improve the capacity for study of the summed or individual effects of different time scales. This time scale consideration resulted in a more physiological approach to modeling the cardiovascular system than previous models. The time scales modeled were an acute seconds-to-minutes scale, during which the baroreflex acts, and a minutes-to-hours scale during which blood volume control occurs. The model was then optimized to allow for future coupling to computationally expensive growth and remodeling models. Arterial pressure regulation was demonstrated in both normal conditions and the pathophysiological condition of aortic valve disease. The work of this thesis successfully reproduced the local effects of the disease, and demonstrated the physiologic response on multiple time scales to the reduction in arterial pressure at an aortic stenosis.

Chapter 1: Background

1.1 Cardiovascular Anatomy & Physiology

The primary purpose of the cardiovascular system is to transport essential nutrients to and remove metabolic waste products from the multitudinous tissues of the body. These molecules are transported by the blood through a system of arteries, arterioles, capillaries, venules, and veins. The heart is the pump which drives the movement of blood so that this transport can occur. One of the primary nutrients being delivered to the tissues of the body, as well as to the heart itself, is oxygen. The heart consists of four chambers: the left and right atria and ventricles. The right side of the heart is responsible for receiving deoxygenated blood from the veins of the body, and pumping it through the pulmonary arteries to the capillaries of the lungs. There, the blood is oxygenated and delivered by the pulmonary veins back to the left atrium of the heart. The left atrium transports blood to the left ventricle of the heart, which pumps oxygenated blood to the entire body through the aorta and the rest of the systemic arterial system.

The heart's pumping mechanism can be generally described as muscular contractions that generate pressure differentials to move blood through the circulatory system. The four valves within the heart function to create unidirectional flow. The two atrioventricular valves that separate the atria and ventricles are the mitral valve (LA to LV) and the tricuspid valve (RA to RV). The two semilunar valves that separate the ventricles from the outflow tracts are the pulmonary valve and aortic valve. When the pressure differential across a valve changes direction, the valve either opens to allow blood to exit or closes to prevent backflow. This pressure differential is generated by the contraction of cardiomyocytes, the specialized muscle cells of the heart. These

muscle cells are joined together by intercalated discs, allowing the heart to contract synchronously as a functional syncytium.

When action potentials are triggered by the pacemaker cells of the sinoatrial node on the right atrium, an electrical impulse travels across the atria, causing the cardiomyocytes to be depolarized and contract in a progressive manner towards the apex. This results in blood being ejected from the atria into the ventricles. Then, the electrical signal is slowed down at the atrioventricular (AV) node, travels to the bundle of His, is transmitted down the left and right bundle branches, and ultimately travels along the Purkinje fibers. The delay at the AV node after atrial stimulation allows for the ventricles to fill with blood while the impulse travels to the Purkinje fibers. The Purkinje fibers then transmit the electrical signal to the ventricles so that they contract and eject blood out of the heart. In summary, the heart is a coordinated electrical and mechanical organ that performs the pumping action required for continuous blood flow throughout the body.

1.1.1 The Cardiac Cycle

The two phases of the cardiac cycle are referred to as systole and diastole. Systole is the phase during which the ventricles are activated and eject blood into the pulmonary and systemic arteries. Specifically, it is the period of the cardiac cycle following ventricular filling and lasting until the end of ejection. Within systole, there are two distinct phases. First, isovolumetric contraction occurs, during which the aortic valve remains closed, but pressure is building as the ventricles begin to contract (Figure 1.1 B). Next, the aortic valve opens and ejection occurs (Figure 1.1 C). Diastole is the period during which the ventricles are inactivated, and is defined as the time

following ejection up until the end of ventricular filling. Diastole also has two phases. The first phase is isovolumetric relaxation, during which pressure is falling within the ventricles, but the AV valves remain closed (Figure 1.1 D). Once pressure in the ventricles falls below the pressure in the atria, the AV valves open, and the ventricles fill with blood (Figure 1.1 A). This results in a slight rise in pressure prior to the onset of systole. The pressure-volume relation, or PV curve, for one cardiac cycle is frequently studied and reported, and Figure 1.1 below represents an idealized PV curve.

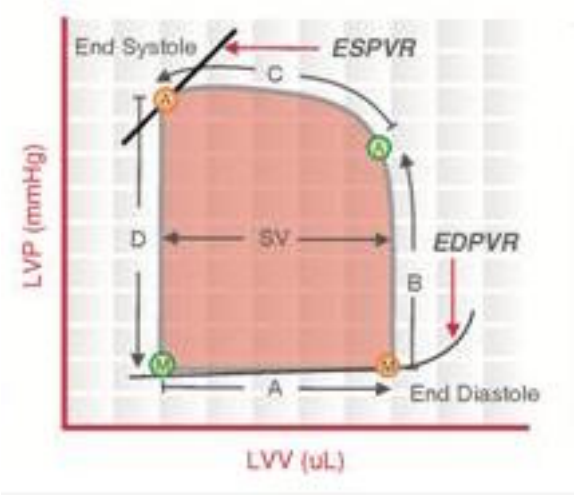

Figure 1.1. Left Ventricular Pressure-Volume Curve. **A**. Diastolic Filling. **B**. Isovolumic Contraction. **C**. Ejection. **D**. Isovolumic Relaxation. ESPVR = End-Systolic Pressure-Volume Relationship. EDPVR = End-Diastolic Pressure-Volume Relationship. SV = Stroke Volume. Green M- Mitral Valve Opens. Orange M- Mitral Valve Closure. Green A- Aortic Valve Opens. Orange A- Aortic Valve Closure. (Source: Wikimedia Commons [5])

1.1.2 Time-Varying Elastance

The instantaneous slope of the pressure-volume relationship is termed the elastance, which is maximal at end-systole (ESPVR) and minimal at end-diastole (EDPVR). When the elastance is found for each point of the cardiac cycle, the time-varying elastance curve is the result. The rise in elastance from diastole to systole can

be seen in Figure 1.2 below. Similarly, the left-ventricular elastance falls as the ventricle returns to its relaxed state.

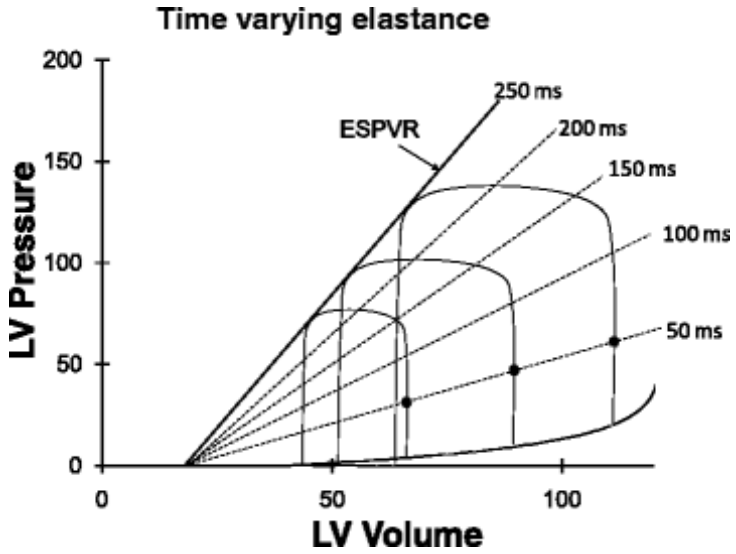

Figure 1.2. Time-Varying Elastance. (Source: Walley, K. CC BY SA 3.0 [35])

1.1.3 Ventricular-Vascular Coupling

An important aspect of cardiovascular function is the interaction between the heart and the vasculature. This is commonly analyzed using the end-systolic elastance (E_{es}) and arterial elastance (E_a). The arterial elastance concept was first developed by Suga and Sagawa, to represent the arterial stiffness [33]. The effective arterial elastance was shown empirically to follow the relation: $E_a = ESP/SV$, which is the negative slope of the line from the end-systolic point to the end-diastolic volume point on the volume axis. The intersection of this line with the ESPVR is the end-systolic point. E_{es} and E_a represent the mechanical characteristics of the physically coupled ventricles and arteries, which provides some insight into how they will interact. Optimal coupling has been found to occur when the ratio of E_a to E_{es} is approximately equal to 1 [33,6]. If arterial function declines, such as with aortic stenosis or stiffening of the

arterial wall, the ratio increases, representing ventricular-vascular decoupling. Thus, the relation E_a/E_{es} is a useful tool for quantifying cardiovascular functionality.

1.2 Blood Pressure Regulation and the Baroreflex

Arterial pressure reaches a maximum at end-systole and a minimum at end-diastole. Mean arterial pressure (MAP) is the average pressure in the large arteries over the time course of one representative cardiac cycle. Blood flow is the result of the pressure generated by the atrial and ventricular contractions described previously. A commonly used equation to describe the relation between pressure and flow rate is the Hagen-Poiseuille's Equation, or Poiseuille's Law, of fluid dynamics. This law assumes laminar flow of an incompressible, Newtonian fluid through a rigid tube of a constant cross-sectional area. These properties were assumed to hold true for blood flow in the cardiovascular system for this study. The law states that flow rate (Q) is proportional to the magnitude of the pressure gradient (ΔP) and the inverse of the resistance to flow (R).

$$Q = \frac{\Delta P}{R} \qquad (1.1)$$

$$R = \frac{8\eta l}{\Pi r^4}$$

Resistance is proportional to the viscosity of the fluid (η) and the length of the tube (l), and inversely proportional to the radius (r) raised to the fourth power. In the context of the cardiovascular system, Equation 1.1 is used to define a simple equation for MAP:

$$MAP = CO * SVR \qquad (1.2)$$

CO is the cardiac output, and SVR is the systemic vascular resistance. Cardiac output is defined as the quantity of blood volume pumped by the heart in a given amount of

time. It is equivalent to the product of the stroke volume (SV) and the heart rate (HR). However, in the vascular system, arterial capacitance is a significant contributor to the mean arterial pressure as well. Rather than being an ideal resistor, the arterial system is better represented as an impedance, which has capacitive and resistive components.

MAP is one of the many quantities in the human body that is controlled by negative feedback. Rather than being a fixed quantity maintained by homeostasis, blood pressure regulation is dynamic and contains regulatory mechanisms on multiple time scales. It fluctuates as the oxygen demand of the body fluctuates. For example, an increase in physical activity results in decreased parasympathetic nervous stimulation and increased sympathetic nervous system stimulation as a response to increased skeletal muscle O_2 demand. MAP is increased in seconds to minutes, and remains elevated for the duration of the physical activity. In a state of rest, the parasympathetic nervous system dominates, resulting in a lower MAP. Osmoreceptors in the body detect blood osmolarity to contribute to the control of MAP and maintenance of blood pH balance. The renin-angiotensin-aldosterone system plays a key role in regulation of blood volume and osmolarity on a time-scale of minutes to hours, which will be discussed in great detail later. Through numerous mechanisms, the control system for regulation of arterial pressure ultimately alters CO or SVR to meet the nutrient demands of the body. In a healthy, properly functioning cardiovascular system, the MAP is maintained near a set point by multiple feedback mechanisms. Although different for every individual based on their anatomy and physiology, MAP for an average adult is in the range of 70-105 mmHg [10,24].

1.2.1 Introduction to the Baroreflex

The sensors in the cardiovascular system that detect MAP are the baroreceptors. Baroreceptors are sensory neurons that transduce stretch into electrical signals to inform the central nervous system (CNS) of changes in blood pressure. The arterial baroreceptors are located in the aortic arch and the carotid arteries. There are also low-pressure sensing baroreceptors in the large systemic veins, pulmonary vessels, and the walls of the heart. When a blood vessel with baroreceptor nerve endings changes diameter due to a change in blood pressure, the baroreceptors transduce the change in pressure, detected as stretch, into an altered neural firing rate [4]. Increased arterial stretch leads to an increase in baroreceptor firing rate, and a decreased arterial pressure leads to a decreased baroreceptor firing rate. The altered firing rate of action potentials is transmitted to the CNS via the afferent pathway: along the glossopharyngeal nerve from the carotid arteries and the vagus nerve from the aortic arch. This signal arrives at the CNS and is processed at the nucleus of the solitary tract in the brainstem. A negative feedback system is used to transmit a signal via the autonomic nervous system resulting in the opposite effect on blood pressure, thus completing the negative feedback response.

1.2.2 Baroreflex Effectors

The efferent pathway of the baroreflex targets the effector organs that counteract the change in arterial blood pressure. The postganglionic sympathetic nerves synapse on the SA node and AV node of the heart to increase the heart rate, on the ventricular myocardium to increase the contractility of the heart, and on the walls of blood vessels to cause vasoconstriction. They also synapse on the juxtaglomerular

apparatus of the kidneys to stimulate the renin-angiotensin-aldosterone system, which will be discussed in a later section [18]. The contractility of the heart affects the amount of force generated during ventricular contraction, and as a result, the stroke volume. Vasoconstriction of the arterioles increases systemic vascular resistance, and vasoconstriction of the veins causes increased venous return to the heart, which increases stroke volume. The primary neurotransmitter released by the postganglionic sympathetic fibers is norepinephrine. Although there are many other physiological effects of the sympathetic nervous system, these are the pathways most directly related to the change in arterial blood pressure induced by the baroreflex. The parasympathetic pathway counteracts these effects when MAP is detected to have increased. Its primary neurotransmitter is acetylcholine. As described, the baroreflex affects the heart rate, stroke volume, and systemic vascular resistance. Therefore, by Equation 1.2, the mechanisms of the baroreflex affect MAP.

1.2.3 Baroreceptor Properties

There are two types of carotid sinus baroreceptors, with different discharging patterns, according to Seagard, et al. Type I (or A) fibers have a discontinuous, hyperbolic discharge pattern with a high threshold frequency, and are myelinated. Type II (or C) fibers have a continuous, sigmoidal discharge pattern with a lower threshold frequency, and are unmyelinated. Due to myelination, Type I has a faster conduction velocity, in the range of 2-40 m/s. Type II has a slower conduction velocity in the range of 0.5-2 m/s [26]. Type I is thought to provide information about rapid changes in arterial pressure with a high sensitivity above its relatively high threshold pressure. Type II is thought to provide information to the CNS about baseline arterial pressure,

due to its lower sensitivity and threshold pressure [32]. Type I and Type II also have disparate firing frequency ranges, which most likely aids in parsing of the signals in the CNS. Together, Type I and Type II carotid arterial baroreceptors play a vital role in the cardiovascular system's response to a change in arterial pressure. Baroreceptors also have the property of saturating at some maximum firing frequency. This has been reported be in the range of 100-180 Hz, but varies by species and animal [28]. Thus, in modeling, baroreceptor activity is often normalized such that its maximum is 1.

Even with baroreceptors firing at their maximum frequency, the baroreflex is not a 100% efficient system for restoring blood pressure to baseline levels. For any change in arterial pressure, the baroreflex can be approximated to compensate for a maximum of 65-75% of the change [9]. They are also thought to not be the body's mechanism for long-term control of arterial blood pressure [7, 27]. Baroreceptor adaptation occurs during sustained pressure differentials, and is characterized by an altered "set point" of arterial pressure, or the arterial pressure at which the baroreceptors do not trigger an autonomic response. Partial baroreceptor adaptation, also called resetting, has been shown to take place after a pressure differential over a period of approximately 10 to 20 minutes [7,8,9]. Adaptation continues over pressure differentials lasting even longer, reaching maximum adaptation at around 1-2 days [9,16,19]. The baroreceptors then respond to changes about the new set point. Although not thought to be the cause of hypertension, this allows non-normotensive conditions to occur. Baroreceptor resetting and inefficiency mean that other physiological effects and mechanisms for regulation of blood pressure must be necessary.

1.2.4 An Introduction to Blood Volume Control

On a longer time scale than the baroreflex, roughly the scale of minutes to hours, blood volume control enacted by the renin-angiotensin-aldosterone system (RAAS) is one of the main physiological mechanisms for regulation of arterial pressure. The RAAS uses the interaction of specific hormones to regulate blood volume and consequently, arterial blood pressure. The first hormone in the pathway, renin, is produced when prorenin is converted into renin by the juxtaglomerular cells of the kidneys. Renin is an enzyme that converts angiotensinogen into angiotensin I. Angiotensin I is then converted into angiotensin II in the presence of angiotensin-converting enzyme. Angiotensin II acts on numerous effectors to increase arterial pressure (see Figure 1.2 below). It is a potent arteriolar vasoconstrictor, it causes the release of aldosterone from the adrenal cortex, it is antinatriuretic, it provides positive feedback to the sympathetic nervous system, and it causes the secretion of anti-diuretic hormone (ADH) from the pituitary gland.

Aldosterone is a steroid hormone that affects the pressure-diuresis relationship in the kidneys and increases the amount of sodium and water retention. This has the effect of increasing blood volume and blood pressure. ADH acts on the collecting duct cells of the kidney to increase water reabsorption, and also has vasoconstrictive effects on the peripheral vasculature. In sum, the downstream effects of the production of angiotensin II by the RAAS all increase arterial pressure.

One of the three main stimuli of the RAAS is a reduction in glomerular filtration rate (GFR), and the resulting decreased sodium concentration sent to the macula densa. The macula densa responds to a decreased sodium concentration by signaling an increase in renin secretion. GFR is decreased when the glomerular filtration pressure is decreased. Glomerular filtration pressure can be decreased by constriction

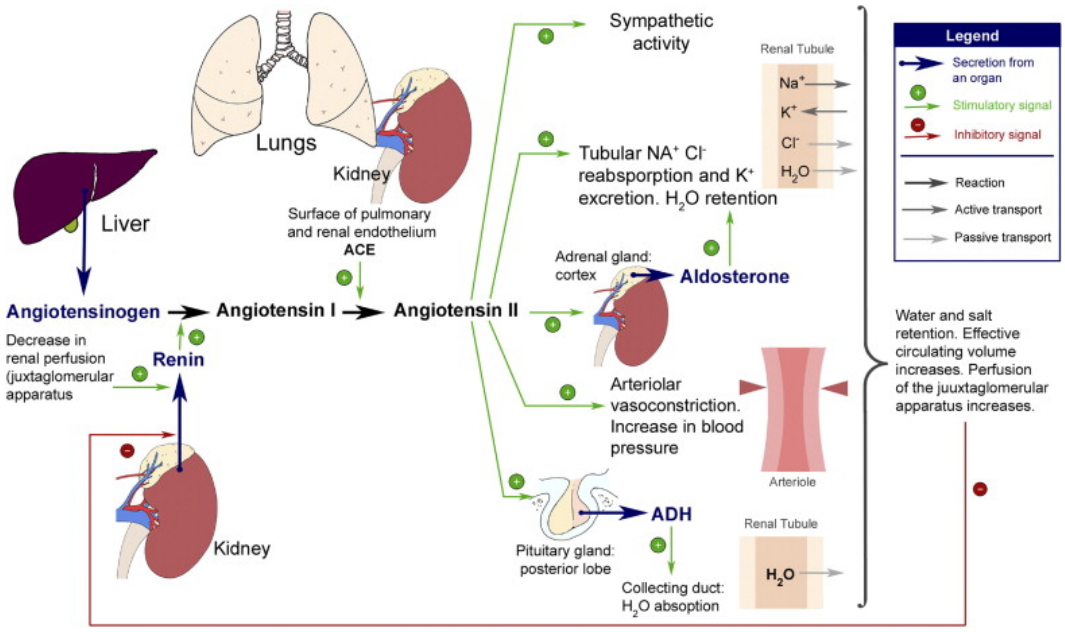

Figure 1.3. The Renin-Angiotensin-Aldosterone System. (Source: Kahn, S. L., Angle, J. F. "Adrenal Vein Sampling", 2010. Reused with permission [15])

of the afferent renal arterioles, dilation of the efferent renal arterioles, or a systemic decrease in arterial pressure. Constriction of the afferent renal arterioles, can be brought about by increased renal sympathetic nerve activity, which receives input from baroreceptors throughout the body. The second stimulus to the RAAS occurs when intrarenal baroreceptors detect a decrease in pressure and then directly signal to the juxtaglomerular cells to release renin. Thirdly, renal sympathetic nerve activity also directly stimulates the juxtaglomerular cells to release renin. These mechanisms all work in parallel to regulate fluid balance and blood volume in the body.

1.3 Existing Cardiovascular Models

For as far back in history as physiology has been studied, researchers have worked to develop models of the cardiovascular system that are physiologically representative, functionally informative, and practically useful. A myriad of different

approaches have been taken, from systems approaches, to mechanical approaches, to electrophysiological approaches. It can be argued that no model will ever be able to fully encompass the vast complexity of the cardiovascular system, so in the application of a model one must carefully scrutinize its limitations. It is important to consider what physiological scale one is attempting to model, and whether adding additional scales could be informative to the problem being addressed. As advancements are made in computational power, more of this complexity can be modeled more accurately without losing practicality. As scientific knowledge is expanded and more is elucidated regarding physiological relationships, biochemical interactions, etc., the scientific accuracy of models can be improved. Thus, there is great room for improvement in the field of cardiovascular computational models, and the goals of creating accurate models of disease and patient-specific models for improved diagnosis and therapy are approaching feasibility.

1.3.1 Lumped-Parameter Circulatory Models

In general, the mathematical approach of using a finite set of parameters and discrete entities to represent a complex, infinitely divisible system is the definition of a lumped-parameter model. This method has been utilized in modeling the circulatory system in what is called the Windkessel model. This model was originally developed by Otto Frank in 1899, and considers a time-dependent electrical analogy for the circulatory system [37]. The simplest of these models, the two-element Windkessel model, accounts for total arterial compliance, which is represented as a capacitance, and total peripheral resistance, represented as a resistance. Frank modeled the time constant of decay in ascending aorta diastolic pressure as the product of this

resistance and compliance. To better represent systole and pulse wave transmission, three-element Windkessel models introduced the characteristic impedance of the aorta. Four-element Windkessel models additionally account for arterial inertance, which plays a role at low frequencies [37]. The overall purpose of using a Windkessel model is to capture some of the viscoelastic properties of arteries in approximating flow through the arterial system, and thus explain the relatively steady flow in the circulation.

Windkessel models have since been modified to additionally account for wave travel, rather than modeling pressure changes in each compartment simultaneously. One type of modified Windkessel model is the “distributed model” that divides up the circulatory system into segments and models the circulatory system as a closed-loop. Then, the propagation of the pressure wave through the vessels is modeled, using conservation of mass and momentum. Closed-loop distributed models have been developed since the early 1960s, often with over one hundred compartments used to represent the arterial tree alone [36].These models have been able to represent ventricular and aortic pressure curves quite accurately [12]. They have been very useful in the study of local flows and pressures, in which case the distribution of pressure and volume throughout the circulation is critical.

Since there is a tradeoff between accuracy and complexity, and the large number of physiological parameters required to be known make this method difficult to validate, models with fewer compartments are sometimes preferable. In the model of William Santamore and Daniel Burkhoff, a four-compartment modified Windkessel model is used to represent the systemic and pulmonic circulatory systems [31]. Also, distributed models that account for wave propagation often require partial differential equations, which are more difficult to solve mathematically. In lumped-parameter

models, spatial distribution is assumed to be one-dimensional, and instead only variation with respect to time is modeled. For example, the Hagen-Poiseuille equation (Equation 1.1) can be used to compute the flow and pressure in the different compartments of the circulatory system. This method is often useful when the focus of the study is on the heart, rather than smaller vessels, and so the level of accuracy needed in the model of the circulatory system is lower.

1.3.2 Baroreflex Models

For short-term regulation of arterial pressure, particularly, the seconds-to-minutes time scale, the baroreflex is the primary system to model. In creating a model of the baroreflex, the different components described in section 1.2 must be considered. The affector pathway, in which the baroreceptor firing rate responds to a change in arterial pressure, is the first necessary component. Then, the effect within the central nervous system should be considered. Finally, the response of baroreflex effectors must be modeled.

One model which attempted to do just this, and represent the baroreflex mathematically, was that of J.T Ottosen in 2000 [27]. This model contains a nonlinear ordinary differential equation (ODE) system for modeling the change in firing rate as a function of the time derivative of the change in arterial pressure. It has a maximal firing rate, time constants to represent baroreflex adaptation, and weighting constants for different types of baroreceptors. It improves on previous models by incorporating baroreceptor nonlinear properties cohesively rather than modeling them independently. The effectors modeled are heart rate, contractility, and peripheral resistance. They are each modeled as sigmoidal decreasing functions of baroreceptor firing rate. Although

each effector function was parameterized separately, not much consideration seems to be taken into the physiological behavior of each of these effectors individually. Therefore, this model may be an oversimplified representation of the baroreflex in the cardiovascular system, although qualitatively it is fairly valid.

Another model of the baroreflex is that of Kun Lu et al., described in their 2001 paper, which includes cardiopulmonary interactions [20]. Similar to Ottosen and many others, the effectors of this model are heart rate, contractility, and vasomotor tone. The sympathetic tone increases ventricular contractility through a proportional increase in the end-systolic elastance of the heart. This was described in section 1.1.2. The heart rate is a second-order function of both sympathetic and vagal frequencies, and is modeled after the method of Sunagawa [34]. Arterial resistance is related exponentially to the sympathetic tone. This equation did not seem to be validated or explained. This model also included a pulmonary model, modeling gas exchange at the lungs, and the effect of pleural pressure on the cardiovascular system. The cardiopulmonary interactions of this model allow for accurate modeling of the Valsalva maneuver. However, the extent of validation of some of the components of the baroreflex model was minimal. The results for ventricular and aortic hemodynamics matched what would be expected for a normal case, but the baroreflex was not validated in test cases, and any longer term effects were not taken into account.

In more recent models by Daniel A. Beard, a more thorough approach to modeling the system-wide baroreflex response was taken [3]. In Beard's model of baroreflex afferent firing, firing rate is a function of the rate of change in strain of the arterial wall, rather than the change in pressure directly. The strain is calculated based on the change in aortic volume. The change in aortic volume is modeled as a function

of the change in aortic pressure and the compliance of the vessel wall, and also takes into account the viscoelastic properties of creep and stress relaxation. The model for baroreceptor firing rate incorporates saturation and nonlinear activation properties. The change in baroreflex firing rate is then related to the change in sympathetic tone. The effector pathway of the baroreflex is modeled as the effect of sympathetic tone on the contractility of the heart, the heart rate, and the total peripheral resistance. These effectors all have a different modeling approach based on their physiological mechanism. The change in ventricular contractility is modeled as a change in the time-varying elastance. It is simulated using a sinusoidal function that increases the maximum elastance with increasing sympathetic tone. For total peripheral resistance, the sympathetic tone contributes to a change in arterial resistance. The heart rate is increased as a first-order function of sympathetic tone. In this way, Beard et al. have created a baroreflex model that better approximates the physiological response of the system. They parameterized the model using experimental data as much as possible, and the results appear to fit experimental data well for baroreflex responses to both hemorrhaging and volume infusion cases.

1.3.3 Long-Term Arterial Pressure Regulation Models

On longer time scales, the baroreflex is insufficient in regulating arterial blood pressure, as described previously. Instead, the renin-angiotensin-aldosterone system and its associated mechanisms are thought to be the key players in regulating arterial pressure on the scale of minutes to hours. In 1972, Arthur Guyton and colleagues published a computational model of long-term blood pressure control [14]. This model introduced the concepts of autoregulatory local controls, as well as the pressure-

natriuresis relationship in blood pressure control, which were relatively novel concepts at the time. It is based on the core tenet that the kidneys are the primary regulators of long-term arterial pressure. The Guyton-Coleman model contains a large number of other physiologic mechanisms, and conceptually, it has contributed a great deal to understanding long-term regulation of arterial pressure and the connection between sodium balance and blood pressure. However, its complexity has been a hindrance to its usability. The Guyton-Coleman model has been highly influential in understanding the long-term control of arterial blood pressure, but is lacking in transparency and practicality. Additionally, new information regarding long-term blood pressure control has been developed since 1970s, so more updated models may be preferential.

A more recent model by Viktoria Averina et al. focused on long-term adaptation of the pressure-natriuresis relationship that is central to the Guytonian model [1]. The aim of this model was to elucidate the etiology of hypertension, and to take into account the possibility that neural inputs—mainly sympathetic stimulation of the vasculature—could be the source of hypertension rather than pressure-natriuresis dysfunction. The model incorporates pressure-independent natriuresis, or sodium balance that is dependent on sodium intake rather than on arterial pressure. This is divergent from the assumption of the Guyton-Coleman model that pressure-natriuresis dysfunction is the only possible cause of hypertension, and thus, the only long-term regulator of arterial blood pressure.

In another model developed by Daniel Beard, both the neural inputs of the autonomic nervous system and the pressure-natriuresis relationship were taken into account. In a highly transparent model, arterial pressure is regulated on the scale of minutes to hours by the kidneys. Sympathetic tone and MAP contribute to the rate of

release of renin, which has cascading effects through the renin-angiotensin-aldosterone system. Specifically, renin release is directly related to angiotensin II release, as was found to be the case *in vivo*. Angiotensin II release is then related to a shift in the pressure-natriuresis relationship, which affects the rate of volume output via the kidneys [3]. Angiotensin II levels also affect the arterial resistance to model its vasoconstrictive effects. In addition, whole-body autoregulation is included in the regulation of arterial resistance. The tests run on this model matched well with experiments by Guyton et al. for the response to volume infusion, and also compared well to empirical data for the response to hemorrhage. Beard's model improved on previous models in that it included a model of chronic baroreflex adaptation. It was used to test an alternative hypothesis for primary hypertension etiology to that assumed by Guyton and others that renal dysfunction is the primary contributor. The hypothesis tested was that arterial stiffening may be sufficient to result in long term dysfunction of arterial pressure regulation, which required a modification of how baroreceptors were modeled. In sum, Beard's model contains mechanisms for both renal inputs and neural inputs in long term arterial pressure regulation, and represents a highly robust system.

1.3.4 Time-Varying Elastance Models of the Heart

As described in section 1.1, the main function of the heart is to convert mechanical energy into pressure that generates flow of blood through the circulatory system. Lumped parameter models of the heart have been created to model the time-varying relationship between pressure and volume in the ventricles using the time-varying elastance discussed in section 1.1.2. In time-varying elastance models of the

heart, ventricular pressure can be approximated as volume changes over time, the using the relation:

$$P(t) = E(t) [V(t) – V_o] \quad (1.3)$$

V_o is the unloaded volume of the ventricle, which is approximated by finding the intersection of the EDPVR or ESPVR with the x-axis, where LV pressure is 0 mmHg. This relation applies for most of the cardiac cycle, except during the time periods of approaching end-diastole and early systole where there are non-linearities. It has been shown empirically that the ESPVR is a linear relation, while the EDPVR is often modeled using an exponential relationship. One example of a time-varying elastance model of the heart is that of Santamore and Burkhoff, which uses Equation 1.4 to find end-systolic pressure, and Equation 1.5 for end-diastolic pressure [31]. The time-varying elastance model used to describe the instantaneous pressure-volume relationship is shown in Equation 1.6 below.

$$P_{es} = E_{es} (V_{es} – V_o) \quad (1.4)$$

$$P_{ed} = B [e^{A(V_{ed} - V_o)} – 1] \quad (1.5)$$

$$P(t) = E(t) (P_{es} – P_{ed}) + P_{ed} \quad (1.6)$$

In Equation 1.5, A is a constant representing exponential end-diastolic stiffness and B is a constant representing linear end-diastolic stiffness. This model allows the time course of pressure to be calculated over the cardiac cycle when the time-varying elastance is defined. It accounts for the non-linear properties of the EDPVR and the time-varying elastance. For a closed-loop circulatory model, this would be coupled to a lumped parameter circulatory model as described in section 1.3.1, where the arterial and venous compartments may make use of Hagen-Poiseuille flow.

1.3.5 Long-Term Growth Models of the Heart

For elevated pressures on longer time scales of days to months, growth and remodeling can take place in the heart and vasculature. Much progress has been made in the area of biomechanical modeling of long-term growth and remodeling. Advanced computational methods like the Finite Element Method (FEM) have been used to model the regionally variable stress and strain distributions in myocardial and vascular tissue. Active and passive material properties of the heart are integrated in these models to create more accurate results than those of empirical relations such as time-varying elastance. In the FEM, the heart is modeled by discretization of its geometry into a finite number of sections, or elements. Boundary conditions and governing equations are applied, and an approximation method solves over the domain. The FEM is a computationally involved method that allows for exceptional 3-D models to be solved. It improves on lumped-parameter models in that regional effects can be modeled. However, it is highly computationally intensive, and while technology is advancing in terms of computational power, it can be advantageous to minimize use of this method.

The finite element method described above is of interest in modeling longer-term growth in cardiac or vascular tissue. In the case of ventricular hypertrophy, a FEM of the heart can be used to simulate a growth response to pressure or volume overload. Pressure and volume overload have been shown to result in compensatory growth in cardiac muscle tissue. In ventricular pressure overload, concentric hypertrophy occurs when sarcomeres, the functional units of striated muscle, are added in parallel to the existing muscle tissue. This results in ventricular wall thickening. In ventricular volume overload, sarcomeres are added in series, which results in eccentric hypertrophy. One group that has developed this type of modeling is

the Cardiac Mechanics Research Group at UC San Diego. A strain-based growth law for cardiac hypertrophy was described in the paper published by Kerkhoffs et al. in 2012 [17]. This growth law was based off of that proposed by Rodriguez et al in 1994, in which the deformation gradient is decomposed into the elastic deformation and plastic growth deformation [30]. Using a FEM of the heart, and the modeling environment Continuity also developed at UCSD, the growth caused when aortic stenosis leads to left ventricular pressure overload was modeled. Vascular hypertrophy is a phenomena in which there is vascular wall thickening and vascular remodeling in response to altered stresses, such as in the case of hypertension [22]. Vascular growth and remodeling has also been modeled with finite element models as well as agent-based models [38]. In order to improve long-term growth models, it is important to lay a foundation with accurate models of shorter-term arterial pressure regulation. The pressures in the circulation are the boundary conditions for these growth models, so although growth modeling was not employed for this thesis, this foundation was laid for future growth modeling.

1.4 Aortic Stenosis

In this study, the physiological changes that occur in the pathological condition of aortic stenosis were investigated for their ramifications in arterial pressure regulation on multiple time scales. Aortic stenosis was chosen due to its well characterized physiological effects in human and animal models, such that the results of the model could be compared to experimental and clinical data. In this section, the etiology and characteristics of the disease, as well as the clinical measures for classifying the

severity of the disease will be presented.

1.4.1 Pathophysiology

Aortic valve stenosis, also called aortic stenosis, is the narrowing of the aortic valve orifice area. The reduced orifice area results in a greater afterload, causing the left ventricle to have to work harder to eject blood into the aorta. Aortic stenosis can be caused by a bicuspid aortic valve, by calcification of the aorta, or by various diseases such as rheumatic heart disease. Normally, the aortic valve is tricuspid. A bicuspid aortic valve is a congenital defect in which two of the valve leaflets are fused together, resulting in a reduced orifice area.

Calcification is the most common cause of aortic stenosis. The exact pathogenesis of calcification in aortic valve disease is still unknown, but it is thought to be similar to the pathogenesis of atherosclerosis. In atherosclerosis, endothelial damage along with pro-inflammatory activity leads to plaque formation. Fatty acid plaque formation is thought to be the result of lipoprotein deposition and subsequent oxidation, which results in macrophage recruitment and accumulation. Calcification occurs when calcium is deposited on the surface of atherosclerotic plaques. Aortic valve lesions have been found to contain lipoproteins, as well as inflammatory markers such as interleukins (IL-1β), tumor necrosis factor (TNF)-α, and matrix metalloproteinases (MMPs) [25]. Thus, aortic valve calcification may be an active process similar to atherosclerosis.

Calcified aortic valves have increased stiffness and prevent the valve from opening as widely. This can result in altered flow dynamics across the valve, leading to a pressure gradient across the valve, and reduced lateral pressure distal to the valve.

The reduced lateral pressure reduces flow to the coronary arteries. The significantly increased afterload in AS results in pressure overload, which leads to ventricular hypertrophy as well as diastolic dysfunction over time. A stenotic valve often does not result in noticeable symptoms until the stenosis becomes very severe. At this point, the condition often has other comorbidities, such as renal dysfunction, coronary artery disease, left ventricular dysfunction, and pulmonary hypertension [11]. When symptoms do present, they often include fatigue or fainting upon exertion, chest pain, heart palpitations, and a heart murmur. This disease usually presents around age 40-50 for a congenital defect, and age 65-75 for the progressive disease [29].

1.4.2 Classifications

The severity of aortic valve disease has been classified according to various clinically measurable parameters. These parameters are the aortic valve area, the transvalvular pressure gradient, and the transvalvular jet velocity. The European Association of Echocardiography (EAE) and American Society of Echocardiography (ASE) have classified aortic stenosis severity according to three categories. These classifications are shown in Figure 1.4 below.

These recommendations indicate that as the aortic valve area decreases, the mean pressure gradient and the aortic jet velocity are expected to increase. However, this is not the always the case, as with low-flow low-gradient severe AS. The peak gradient has also been found to vary according to severity of the AS: 15-40 mmHg for mild AS, 40-70 mmHg for moderate AS, and 70-100 mmHg for severe AS [2].

Recommendations for classification of AS severity[1]

	Aortic sclerosis	Mild	Moderate	Severe
Aortic jet velocity (m/s)	≤2.5 m/s	2.6-2.9	3.0-4.0	>4.0
Mean gradient (mmHg)	-	<20 (<30[a])	20-40[b] (30-50[a])	>40[b] (>50[a])
AVA (cm^2)	-	>1.5	1.0-1.5	<1
Indexed AVA (cm^2/m^2)		>0.85	0.60-0.85	<0.6
Velocity ratio		>0.50	0.25-0.50	<0.25

- [a]ESC Guidelines.[2]
- [b]AHA/ACC Guidelines.[3]

Figure 1.4. Recommendations for classification of AS severity. (Source: Echopedia.org. Available under creative commons license [2])

1.5 Specific Aims

As previously discussed, an ideal model of the cardiovascular system should be physiologically representative, functionally informative, and practically useful. In creating a physiologically representative model of the hemodynamics of the cardiovascular system, numerous control systems must be taken into account. The time scale on which each physiological mechanism operates varies substantially. The baroreflex operates on the scale of seconds to minutes, and responds to acute changes in pressure by altering heart rate, myocardial contractility, and peripheral resistance. Blood volume control operates on a time scale of minutes to hours, in which the kidneys regulate blood pressure by means of the renin-angiotensin-aldosterone system. When pressure is altered on a longer time scale of days to months, growth and remodeling occur in the heart and other components of the cardiovascular system.

In this thesis, a multi-scale model was created to improve the capacity for study of the summed or individual effects of different time scales. First, an arterial baroreflex was modeled on a time scale of seconds to minutes, and arterial pressure regulation was simulated in normal and aortic stenosis conditions. The baroreflex model was

coupled with a lumped parameter model of the circulatory system with beat-to-beat regulation. Next, longer-term arterial pressure regulation as enacted by the RAAS and blood volume control was simulated on a time scale of minutes to hours. These two models of arterial pressure regulation were then coupled for the purpose of studying the effects of different conditions, such as aortic stenosis, on multiple time scales. There is great potential for improved models of the cardiovascular system to be used by researchers and medical professionals in the study of pathophysiological conditions and in generating patient-specific models of cardiac biomechanics.

Chapter 2: Methods

2.1 The Baroreflex Model

The baroreflex model utilized in this thesis was based on that developed by Beard et al. [3]. Beard's model was chosen because it modeled well established effectors of the baroreflex in a robust phenomenological manner and was well validated. The aorta was modeled as a thin-walled cylinder, and a change in aortic pressure with respect to time was related to a strain in the aortic wall, which was transduced into a change in the baroreceptor firing rate. This resulted in a change in sympathetic tone, which affected the physiological effectors of heart rate, heart contractility, vascular tone, and the state of the RAAS. This model was implemented using a series of ODEs in the development environment of MATLAB 2014b [21].

2.1.1 Coupling to a Lumped Parameter Circulation Model

In order to model the hemodynamics of the entire circulatory system, the baroreflex model was coupled to a lumped parameter circulation model. The lumped parameter model used was a six compartment model developed by Santamore and Burkhoff, which uses canine parameters [31]. The six compartments were the left ventricle, right ventricle, pulmonary arteries, pulmonary veins, systemic arteries, and systemic veins. Each ventricle was modeled as a time-varying elastance relation, as described in section 1.3.4. The pressures and volumes in each vascular compartment were solved using Poiseuille's Law and initial conditions for volumes and resistances. The software program used to run the closed-loop circulation model was developed in MATLAB in collaboration with Dr. Kyoko Yoshida at the University of Virginia. It uses a 4^{th} order Runge-Kutta numerical method and iterates until the steady-state condition—

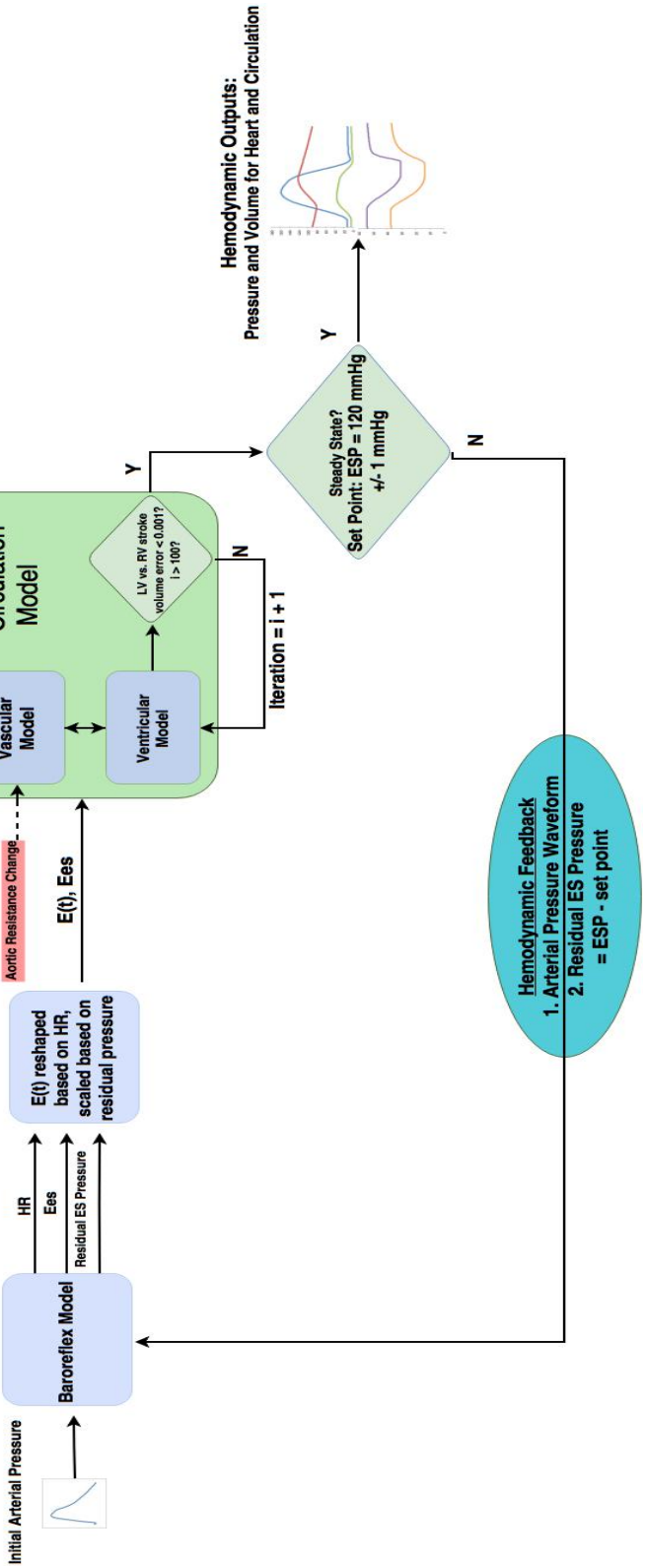

Figure 2.1. Closed-Loop Baroreflex Model.

that the cardiac outputs of the left and right ventricles match within a set tolerance—is met [21]. These iterations are on a beat-to-beat time scale, as the outputs of this model are the pressures and volumes for each of the six compartments over one cardiac cycle.

The coupling of the circulation model and the baroreflex model is shown in Figure 2.1. Within the green box labeled “Circulation Model”, the ventricular model, vascular model, and ventricular stroke volume matching iterations are represented. The outer loop that is connected to the circulation model is the baroreflex negative feedback loop. The outputs of the overall model shown at the right-most side of Figure 2.1 are the hemodynamics of the six compartments, or the pressure and volume time courses for each beat of the baroreflex model.

The baroreflex effects were implemented in the coupled circulation model through the modification of two parameters. When an arterial pressure waveform was input into the baroreflex model developed by Beard, the outputs were an updated heart rate and time-varying elastance. This is the first light blue box of Figure 2.1 labeled “Baroreflex Model”. The maximum value of the time-varying elastance, which is equivalent to the end-systolic elastance, represented a change in ventricular contractility. This change was enacted gradually, since, physiologically, ventricular contractility is not changed instantaneously. This incremental increase in contractility was enacted using the equation below:

$$E_{es}(t) = E_{es_o} + S[1 + \tau_E \frac{residual}{set\ point}] * [E_{es_{max}} - E_{es_o}] \quad (2.1)$$

In this equation, E_{es_o} is the baseline end-systolic elastance. S is a scaling factor that determines the magnitude of increase in E_{es}, and it was set to 0.5. τ_E is a scaling factor

that reduces the rate at which E_{es} is changed, and it was set to 7. The residual is the difference between the current ESP and the set point for ESP. $E_{es_{max}}$ is the new elastance calculated by the baroreflex model. In this way, E_{es} was incrementally increased in a linear fashion as the system approached its steady state. It was also set so that the change in E_{es} was non-negative.

The change in heart rate was applied to the circulation model using the time-varying elastance vector, which is utilized in Equation 1.6; the elastance curve used in the circulation model was reshaped according to the heart rate, such that the duration of the cardiac cycle is set to the time for one beat. The changes in heart rate and end-systolic elastance were calculated in the closed-loop baroreflex model. As shown in the second light-blue box of Figure 2.1, they were then used to update the ventricular model of the circulation model.

Negative feedback was applied so that the end-systolic arterial pressure (ESP) is controlled around a defined set point. As described in section 1.2.3, the baroreflex is only capable of correcting for about 70% of the change in arterial pressure. Thus, the steady-state value is set to:

$$P_{ss} = P_{\Delta} - 0.7*(residual) \tag{2.2}$$

where P_{Δ} is the altered ESP, P_{ss} is the steady-state value reached by this model. This equation defines the end-point, P_{ss}, of the model. In order to reach P_{ss}, the residual of each iteration is used to modify the length of the elastance vector, which represents the heart rate. If the residual is positive, the elastance vector is lengthened to reduce the heart rate, and if the residual is negative, it is shortened to increase the heart rate. This provides negative feedback, as shown in the teal oval of Figure 2.1. This negative feedback was not present in Beard's baroreflex model, and allows the baroreflex

system to be controlled around a user-defined set-point. The model iterates until the baroreflex reaches its defined steady state, which takes place on a scale of seconds to minutes.

2.1.2 Testing the Baroreflex Model

To simulate different conditions, the user is given an option to alter the resistance to flow for any of the six compartments. In order to test the arterial baroreflex, a change in arterial pressure was imposed, as shown in the red rectangle of Figure 2.1. Since the systemic arteries were lumped together into one compartment, the arterial resistance represented the resistance to flow into the systemic arteries from the left ventricle, which was equated to the characteristic resistance of the aorta. The normal value used was 0.11 mmHg*s/ml [31]. The model was then run at numerous increased values of aortic resistance, up to 10x the normal, to represent various levels of severity of aortic valvular disease. As defined by Equation 1.1, a reduced radius is directly related to a greater resistance to flow through that opening. Thus, the magnitude of a change in aortic resistance was related to aortic valve orifice area, which was then used to define the aortic stenosis severity being represented. The results were compared to clinical data for patients with healthy and stenotic aortic valves.

2.2 Renovascular Model

The method used for simulating longer-term control of arterial blood pressure via blood volume control was also based on a model developed by Beard et al. [3]. Decreased MAP was the stimulus for the rate of renin release. The release of renin

stimulated the release of angiotensin II, which resulted in a shift in the pressure-natriuresis curve and a decrease in the rate of volume output by the kidneys. This resulted in an increase in blood volume over time, and consequently, increased blood pressure. One of the RAAS intermediates, angiotensin II, also caused vasoconstriction, which was modeled as an increase in arterial resistance and a decrease in arterial and venous compliance. These two feedback loops are shown in Figure 2.2. This model also incorporated the effects of the baroreflex on the circulation. An increase in sympathetic tone had an increasing effect on the amount of renin released, which ultimately caused a decrease in the rate of blood volume loss and an increase in MAP. Sympathetic tone also directly affected the pressure-natriuresis relationship to result in a decreased rate of volume loss and increased MAP. The resistance and compliance of the arterial system were also affected by the sympathetic tone in addition to the vasoconstrictive effects of angiotensin II. In combination, all of these effectors resulted in long-term regulation of arterial pressure.

2.2.1 Implementation

The input to the renovascular model was the MAP of the baroreflex model steady state. The model was tested by running increased values of MAP that were the outputs of the baroreflex when the arterial resistance was increased, and visualizing the response of the renovascular model. The renovascular model was also run for decreased MAP values. The model was written as a system of ODEs in MATLAB, and solved using the ode23t solver. The set point for MAP was 100 mmHg. The ODEs were parameterized such that the blood volume control occurred on a physiological time scale of minutes to hours.

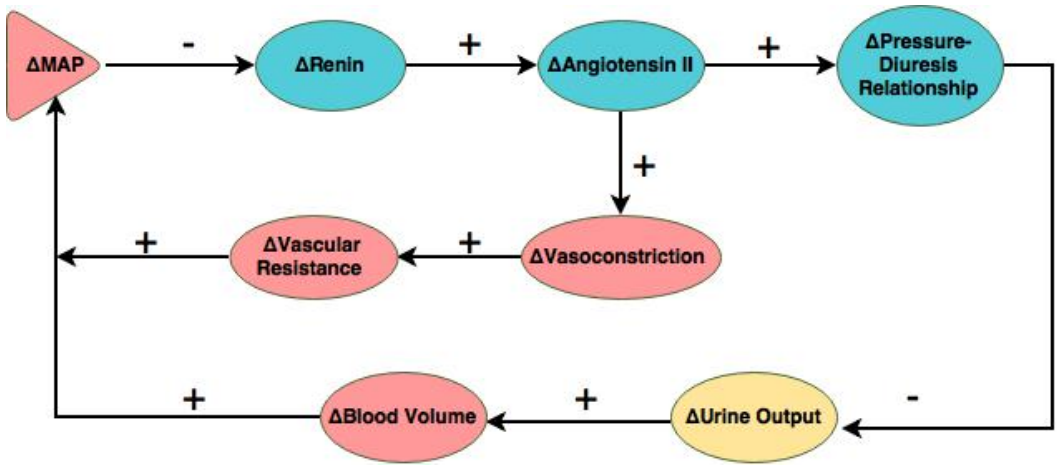

Figure 2.2. Renovascular Model. A plus sign represents a stimulatory signal or an increasing effect, and a negative sign refers to an inhibitory signal or a decreasing effect.

2.3 Optimization

Next, the rate of solving the baroreflex model was optimized. This was in light of the future prospect of modeling growth and remodeling, which takes place on a time scale of days to months. This is shown in the shaded portion of Figure 2.3 below. In order to model this process, a finite element model would typically be used. In this study, the ventricular model used was a time-varying elastance model from the work of Santamore and Burkhoff. In consideration of the potential for coupling the baroreflex model with a computationally intensive model of the heart, the number of iterations of the ventricular model was optimized. Since each baroreflex loop runs a number of ventricular model iterations (see Figure 2.1), the interaction of these two models was optimized. In other words, the total number of ventricular iterations, calculated as the product of the number of ventricular iterations per baroreflex loop and the number of baroreflex loops run to reach steady state, was minimized. This was done through three different methods to attempt to reduce this total. First, the number of ventricular

stroke volume matching iterations was optimized by independently reducing the number iterations run in each baroreflex loop. If the number of iterations was too low, then the deviation from the set point became too large, and the system did not recover to steady state. If the number was too high, then it would reach steady state, but was not optimized. Next, the baroreflex model solving time was reduced, to reduce the number of baroreflex model loops that were run. Finally, this second method was combined with an increased tolerance for both of the steady state conditions of the closed-loop baroreflex model. In this last case, the number of ventricular iterations in each baroreflex loop was variable, rather than fixed, because it was dependent on whether the model had reached its steady state.

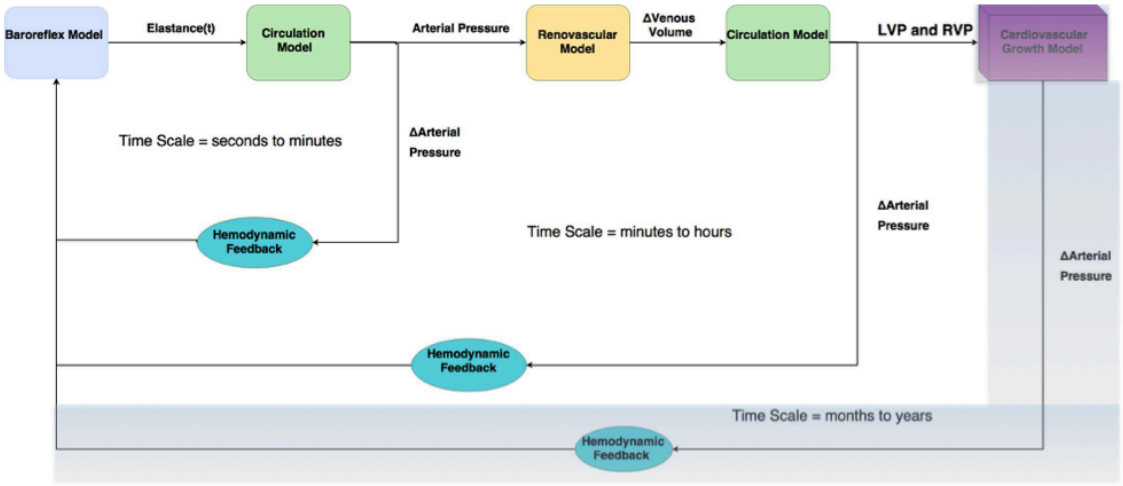

Figure 2.3 Multi-Scale Closed-Loop Circulatory Model.

Chapter 3: Results

3.1 Baroreflex Model Results

A model-generated aortic pressure curve was used as the input to the baroreflex model. This was generated by running an experimental arterial pressure curve supplied by Daniel Beard through the baroreflex model to the set point. The data is shown in Figure 3.1 below, for arterial pressure measured from a spontaneously hypertensive rat (SHR). Data for this rat was measured over 100 seconds, but the first 10 seconds are shown below. Since arterial pressure is significantly higher in rats than in dogs, the baroreflex reduced the arterial pressure in generating the baseline arterial pressure curve. A comparison of the single beat arterial pressure curve of the data and the arterial pressure curve generated by the baroreflex model is shown in Figure 3.2 below.

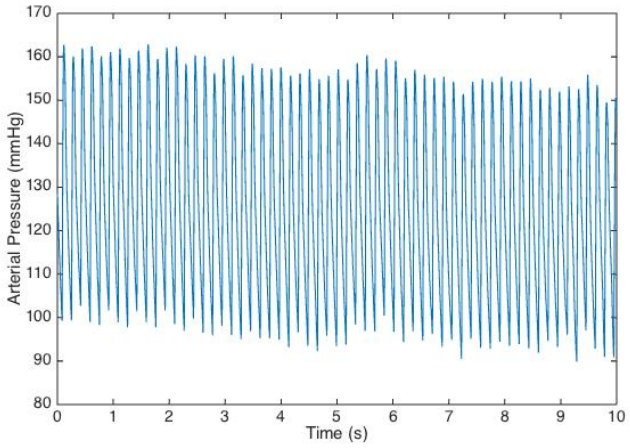

Figure 3.1 Measured Arterial Pressure for SHR. Raw data provided courtesy of Daniel Beard, April 2017.

For the test cases, the aortic resistances used were based on clinical cutoffs for aortic stenosis severity, which are defined according to aortic valve orifice area. These cutoff orifice areas were used to calculate the cutoff aortic resistances according to Equation 1.6. The aortic valve orifice was assumed to be circular.

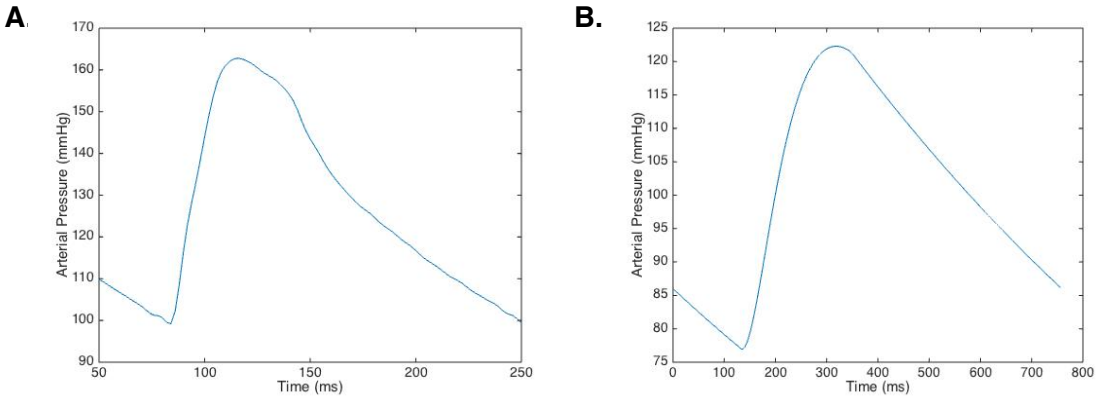

Figure 3.2. Arterial pressure waveforms. **A.** Measured arterial pressure from SHR data for one beat. Data provided by Daniel Beard. **B.** Arterial pressure waveform generated by running the baroreflex model to its set point using the input data from A.

Table 3.1. Aortic stenosis parameters based on recommendations by ESE/ASE [2].

Aortic Stenosis Severity	*Aortic Valve Area (AVA)*	*Percent of normal aortic radius (Δr) Normal = 1.05 cm*	*Aortic resistance (mmHg*s/ml)*
Normal	3.0 cm^2 – 4.0 cm^2	93% – 107%	**0.11**
Mild	1.5 cm^2 – 2.0 cm^2	66% – 76%	**0.33 – 0.62**
Moderate	1.0 cm^2 – 1.5 cm^2	54% - 66%	**0.62 - 1.12**
Severe	< 1.0 cm^2	< 54%	**> 1.12**

Thus, the cutoff aortic resistances are 0.11, 0.33, 0.62, and 1.12 mmHg*s/ml. These aortic resistances were sequentially input into the baroreflex model, and when the aortic resistance was changed to each increased value, the end-systolic arterial pressure decreased acutely. The baroreflex model then responded by decreasing the baroreceptor firing rate, which increased the sympathetic tone, and resulted in increasing heart rate and end-systolic elastance. The baroreflex model reached a steady state when the end-systolic pressure returned 70% of the way to its set point of

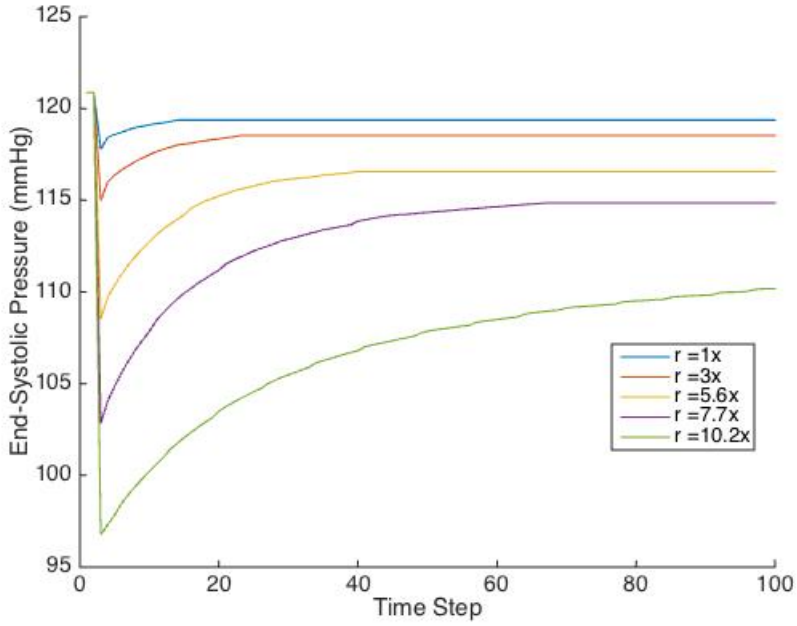

Figure 3.3 End-systolic arterial pressure reaches steady state for five aortic resistances.

Table 3.2 Heart rate at baroreflex steady state for various aortic resistances.

Baseline	***R = 1x***	***R = 3x***	***R = 5.6x***	***R = 7.7x***	***R = 10x***
80 bpm	82 bpm	86 bpm	103 bpm	142 bpm	286 bpm

120 mmHg, as defined by Equation 2.1. Each time step represents one loop of the baroreflex, which is a simulation of one cardiac cycle. The change in heart rate and end-systolic pressure over the course of the baroreflex after acute changes in aortic resistance are shown in Figure 3.1 and Table 3.2 above. The aortic resistances run are defined in the legend according to the proportional increase compared to the baseline aortic resistance of 0.11 mmHg*s/ml. These are the cutoff resistances along with one extra resistance of 0.85 mmHg*s.ml.

The pressure-volume curves for the first time step after the aortic resistance

was set to each of five different values are shown in Figure 3.2. The blue asterisk represents the end-systolic point, which is defined as the time at which left ventricular volume is minimal and represents aortic valve closure. The pressure-volume curves of the final time step of the baroreflex loop, when end-systolic pressure reaches steady state, is shown in Figure 3.3.

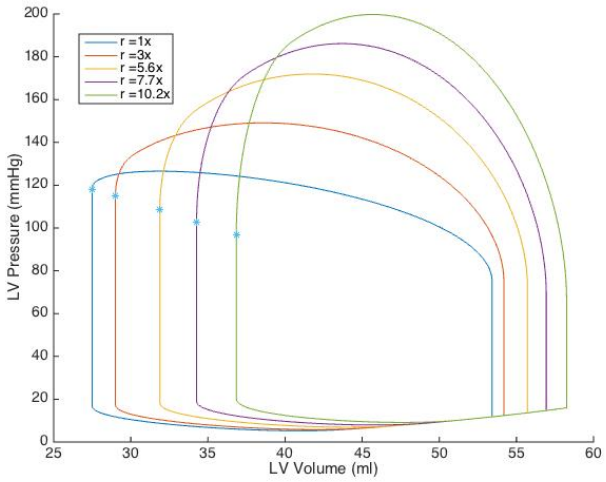

Figure 3.4. Left ventricular pressure-volume curves for altered aortic resistances. Blue asterisk marks end-systolic point.

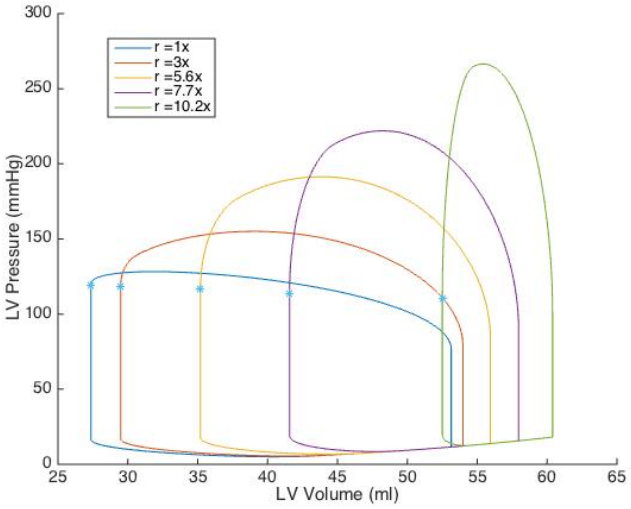

Figure 3.5. Left ventricular pressure-volume curves at the baroreflex steady state. Blue asterisk marks each end-systolic point.

Maximum left ventricular pressure (LVP) increased significantly as the aortic resistance was increased. The maximum LVP increased even further as the baroreflex was enacted. Maximum LVP at the steady state point is plotted as a function of the aortic resistance in Figure 3.4 below. The cutoff aortic resistances for the various levels of aortic stenosis severity are demarcated by the red dashed lines. The maximum LVP has been shown to increase from 120 mmHg up to 260 mmHg in various cases of aortic stenosis, which is matched quite well by the results of this model [13]. The maximum LVP for the normal aortic resistance case was 128.3 mmHg, and the maximum LVP for the cutoff for severe AS was 266.5 mmHg.

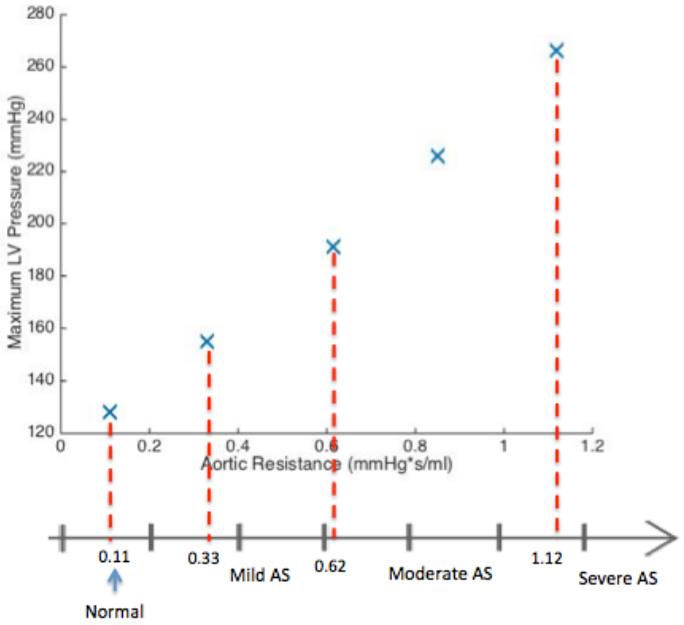

Figure 3.6. Maximum left ventricular pressure for 5 aortic resistances. Red dashed lines from lower axis demarcate cutoffs for aortic stenosis severity categories.

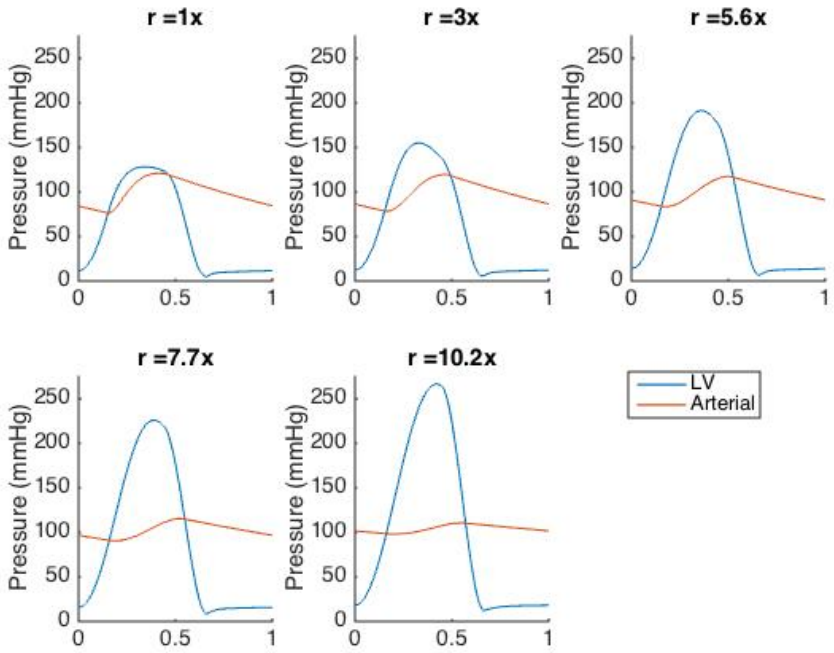

Figure 3.7. Left ventricular and arterial pressure waveforms of the steady state cardiac cycle for five aortic resistances (r).

The left ventricular pressure waveforms are plotted for increasing aortic resistances above. In a perfectly functioning aortic valve, the pressure difference between the two would be zero. It can be seen that the maximum pressure difference between the LV and the aorta increases from a nominal value at r = 1x to over 150 mmHg at approximately 10x aortic resistance. The mean transvalvular gradient is one of the hemodynamic metrics often measured in diagnosing aortic stenoses. It is calculated from the jet velocity measured with Doppler echocardiography. The mean transvalvular gradient was thus compared to clinical data for aortic stenosis, as shown in Table 3.3.

Table 3.3. Mean aortic valve pressure gradient for aortic stenosis severity levels. Predictions by the baroreflex model and the cutoffs recommended by the European Society of Cardiology.

	Normal	***Mild AS***	***Moderate AS***	***Severe AS***
Baroreflex Model Result	< 33 mmHg	33 – 53 mmHg	53 – 78 mmHg	> 78 mmHg
Clinical Recommendations [22]		< 30 mmHg	30 – 49 mmHg	> 50 mmHg

3.2 Renovascular Model Results

For the initial test of the renovascular model, the arterial resistance was increased, in order to model the effects of elevated arterial pressure on renal function. The increased arterial resistance was input into the baroreflex model, and the MAP was calculated at the baroreflex steady state. These MAPs were input into the renovascular model and are tabulated in Table 3.4 below. The MAP for these four values over a simulation time of 300 minutes is shown in Figure 3.6 A. A few of the other intermediates and effectors of the renovascular model were plasma renin levels, the rate of volume output by the kidneys, and the total volume in the circulation. These parameters were tracked over the simulation time and are plotted in Figure 3.5 B-D. From these plots it can be seen that the initial increase in MAP caused a drop in renin and an increased rate of urine output compared to normal, which had the effect of decreasing the total volume in the circulation, and decreasing MAP. The MAP overshot its steady state value, which caused renin to increase and MAP to decrease until it returned to its steady state.

Table 3.4. Mean arterial pressures determined from the steady state of the baroreflex for normal arterial resistance and increased arterial resistances.

R_A (mmHg*s/ml)	MAP (mmHg)
2.7 (normal)	**99.1**
5.4	**112.7**
8.1	**117.4**
10.8	**122.3**

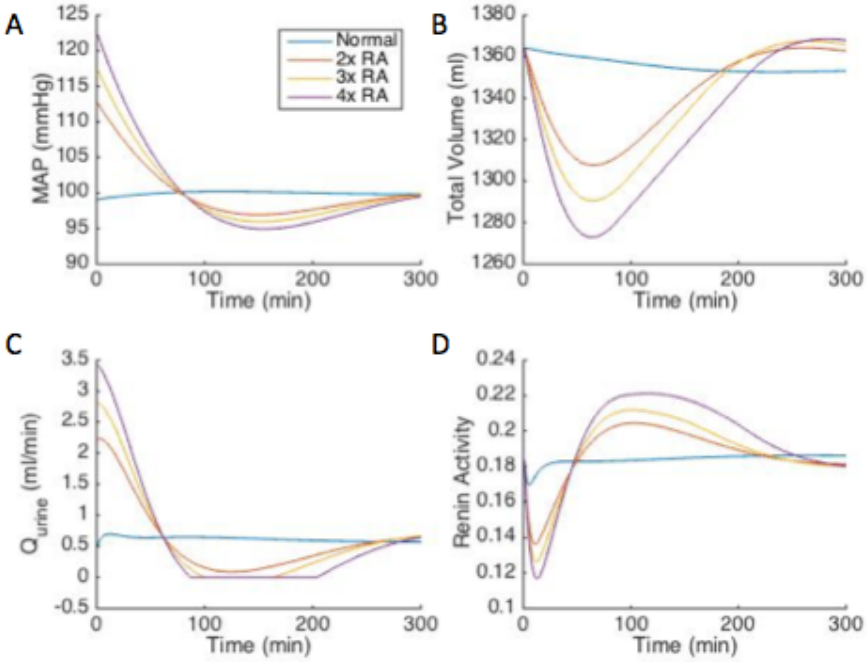

Figure 3.8. Hemodynamic variables vs. time for simulation of the renovascular model at normal and altered arterial resistances according to the legend in A. RA = Arterial Resistance. Q_{urine} = Flow rate of urine.

Next, the renal function curve was compared to empirical data. This was famously studied by Guyton, whose experimental data for sodium output normalized to sodium intake plotted against mean arterial pressure demonstrated the positive dependency of the former on the latter [13]. The renal function curve in terms of volume output normalized to baseline levels that was predicted by the renovascular model of

this thesis is shown in Figure 3.7. The plots of this model are comparable to that of Guyton under the assumption that sodium excretion is proportional to the rate of urine production. For an arterial pressure of 122 mmHg, the normalized rate of urine output was 5.7, whereas for data obtained by Guyton et al. this magnitude of increase in renal output was not seen until about 175 mmHg. Thus, this model may be over-responsive to changes in arterial pressure. The overshoot of the steady state arterial pressure causes the "j" shape of the renal function curve of this model.

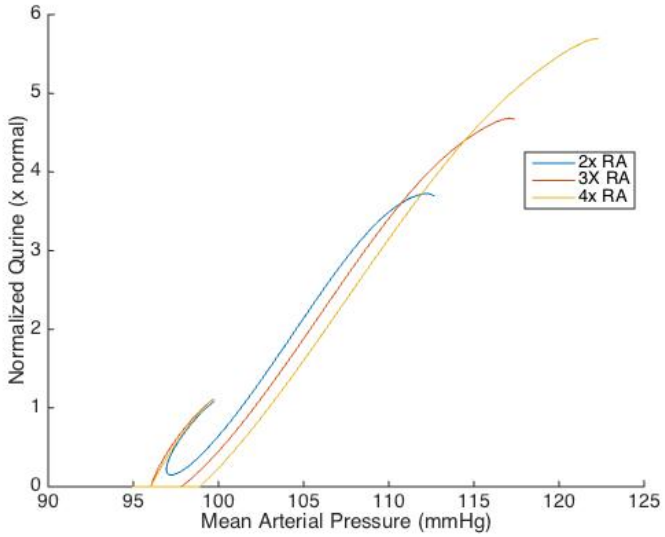

Figure 3.9. Renal output curves predicted by the model of this thesis for three altered arterial resistances—2x R_a shown in blue, 3x R_a in red, and 4x R_a in yellow.

Subsequently, decreased MAPs were run in the renovascular model. These input MAPs were obtained from the results of the baroreflex for a decreased initial MAP due to increased aortic resistance. The aortic resistances used were the aortic stenosis cutoff resistances, and an assumption was made that MAP is only able to recover 70% of the way to its set point of 100 mmHg. The MAPs are tabulated in Table 3.5. The hemodynamic variables that correspond to the renovascular run of these initial MAPs are shown in Figure 3.8. As the magnitude of decrease in MAP was increased, the

increase in renin release also increased in magnitude. This caused an increase in the rate of urine output, an increase in the total volume in the circulation, and thus, an increase in the mean arterial pressure. At higher initial MAPs, there was a greater amount of overshoot, but all cases returned to the set point for MAP after approximately 360 minutes.

Table 3.5. Mean arterial pressures determined from the steady state of the baroreflex for normal aortic resistance and increased values.

Aortic resistance (x normal)	***MAP (mmHg)***
1.0	**99.43**
3.0	**98.55**
5.6	**97.01**
10.2	**93.95**

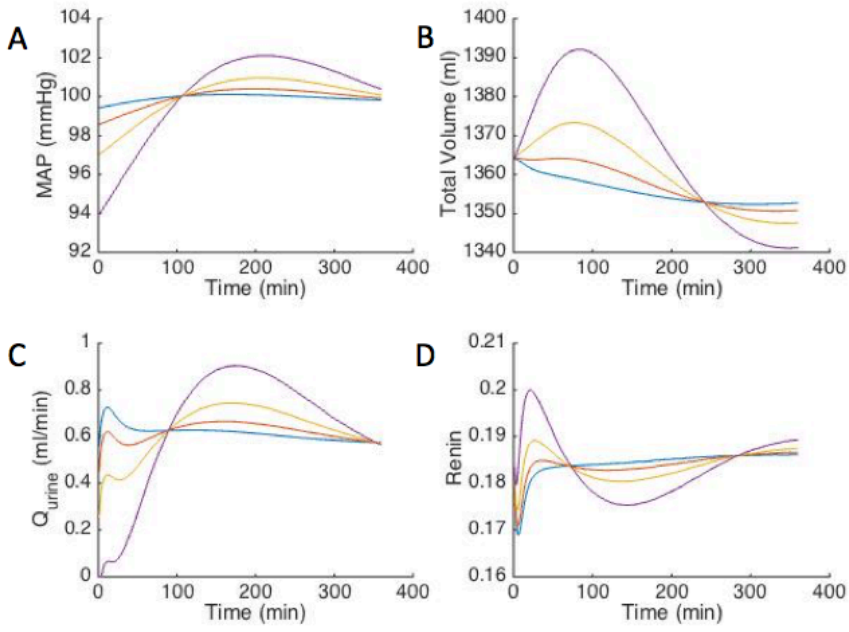

Figure 3.10. Hemodynamic variables vs. time for simulation of the renovascular model at normal and altered aortic resistances. 1x R_{ao} is shown in blue, 3x R_{ao} in red, 5.6 R_{ao} in yellow, and 10.2x R_{ao} in purple.

3.3 Optimization Results

In this study, the ventricular model used was a time-varying elastance model. To model physiological processes on longer-time scales, such as ventricular growth and remodeling, a finite element model of the heart could be used but would dramatically increase the computational time to solve for cardiac function. Thus, the number of iterations of the ventricular model was optimized to maximize the efficiency of this future endeavor. This was achieved using the methods described in section 2.3 above. The results of the baroreflex optimization for the first method of optimization are shown in Tables 3.6 – 3.7 below.

Table 3.6. Optimization of ventricular model iterations within the baroreflex loop for aortic resistance of 0.11 mmHg*s/ml. The most optimal trial is highlighted in green, and the two next most optimal are in yellow.

# ventricular Iterations per BR loop	x # BR loops to solve	= total # iterations
1-4	No solution	**N/A**
5	18	**90**
6	12	**72**
7	10	**70**
8	8	**64**
9	7	**63**
10	4	**40**
11	3	**33**
12	2	**24**
16	1	**16**

Table 3.7. Optimization of ventricular model iterations within the baroreflex loop for aortic resistance of 0.62 mmHg*s/ml. The most optimal trial is highlighted in green, and the two next most optimal are in yellow.

# ventricular Iterations per BR loop	x # BR loops to solve	= total # iterations
1-6	No solution	**N/A**
7	43	**301**
8	30	**240**
9	24	**216**
10	22	**220**
11	20	**220**
12	19	**228**
13	19	**247**
14	18	**252**
15	18	**270**
16	17	**272**
17	18	**306**

The results from these trials of the baroreflex model at set rates of ventricular iterations demonstrate that there is an optimal value at which maximum efficiency is achieved. For the baseline aortic resistance, this was at 10-16 iterations per BR loop, and for 5.6x aortic resistance this was at 8-12 ventricular iterations per BR loop. When running multiple resistances, it is therefore seen that the optimal number of iterations per baroreflex loop to reduce the total number of ventricular iterations run is in the range of 10-12.

For the second method of optimization, the effect of the negative feedback provided by the heart rate, which resulted in the baroreflex model reaching its steady state, was increased by 5x. This resulted in the reduction of the number of baroreflex loops solved as shown in Table 3.8 below. This reduced the total baroreflex model solving time for all five resistances run by about 75%.

Table 3.8. Number of closed-loop baroreflex model steps required to reach steady state before and after optimization of the baroreflex model.

Aortic Resistance	***1.0x***	***3.0x***	***5.6x***	***7.7x***	***10.2x***
Before	12	21	38	71	>102
After	2	3	8	13	30

For the third method of optimization, the tolerance for the baroreflex model steady state was increased from 1 mmHg to 2 mmHg, and the tolerance for the ventricular stroke volume matching was increased from 0.1% to 1%. This reduced the total solving time by an additional 32%. The total number of ventricular iterations for this optimized solution is shown in Table 3.9 below. This is comparable to Tables 3.6 and 3.7, in which the minimal total number of ventricular iterations for 1.0x aortic resistance was 16, and the minimum for 5.6x aortic resistance was 216.

Table 3.9 Total number of ventricular iterations after optimization of the baroreflex model and increased tolerance of the steady state conditions for five aortic resistances.

Aortic Resistance	***1.0x***	***3.0x***	***5.6x***	***7.7x***	***10.2x***
Total # of iterations	12	24	66	216	752

Ultimately, the optimization methods used reduced the total solving time for the closed-loop baroreflex model from about 80 minutes to about 14 minutes.

Chapter 4: Discussion

4.1 Baroreflex Model Results

The results of the baroreflex model for increased aortic resistances were qualitatively comparable to what is measured clinically in cases of aortic stenosis. For greater aortic resistances, the maximum left ventricular pressure increased to compensate for the increased resistance to flow out of the chamber, matching experimental data almost perfectly. The end-systolic pressure decreased due to the reduced ventricular stroke volume. Thus, the pressure gradient across the aortic valve was significantly increased. This is also seen clinically, although not as dramatically as was predicted by this model. This difference was most likely due to the method of determination of the end-systolic pressure point in this model, and simplifications made to the fluid dynamics relations and vascular system. *In vivo*, aortic valve closure is significantly affected by the negative pressure gradient created by a reduction in flow rate towards the end of systole. These inertial effects were not modeled, which caused the end-systolic pressure point to be much lower than would be the case realistically. However, the magnitude of increase in heart rate and heart contractility was realistic, as well as the duration of time that the baroreflex took to recover the arterial pressure to its steady state, which was 10-120 seconds depending on the magnitude of the change.

4.1.1 Baroreflex Model Limitations

The baroreflex model developed was a phenomenological model that primarily focused on changes in macroscopic hemodynamic quantities in the cardiovascular

system as it responded to a deviation from the set point. Accordingly, numerous assumptions were made and limitations existed in using this model. In addition to the lack of inertial effects used in modeling the fluid dynamics in the aorta, the effects of turbulence at a stenosis, and the pulse wave reflections due to arterial branching were not taken into account. These phenomena could have some effect on the hemodynamics in the ventricular and arterial compartments in particular, but they were assumed to be insignificant to the purposes of this thesis. Another limitation was the number of compartments used in the lumped parameter circulation model. In lumping the vasculature into four compartments, a significant amount of ability to model local dynamics and their effect on the heart and circulation is lost. The effect of vasoconstriction in the microvasculature was not considered. Thus, this model is an over-simplification of the physiological ramifications of the baroreflex. Nevertheless, it succeeded in representing the dynamic effects of the baroreflex in the left ventricle and vascular system, which allowed it to be functionally informative.

4.2 Renovascular Model Results

Similar to the baroreflex model, the renovascular model employed in this thesis was a phenomenological model. It modeled the negative feedback of the renin-angiotensin-aldosterone system that contributes to long-term regulation of arterial blood pressure. The controlled variable, mean arterial pressure, was returned to the set point of 100 mmHg within a realistic time frame of approximately 6 hours, as a result of physiologically known mechanisms. However, mean arterial pressure did overshoot its set point, which implies that further parameterization could improve this model's physiological accuracy.

4.2.1 Renovascular Model Limitations

There were a number of limitations to this renovascular model. First, blood volume was assumed to be regulated only by the kidney. Fluid shift at the capillaries, in which volume is lost or retained at the interstitial fluid compartment, was not taken into account. Volume loss through perspiration or any mechanism other than excretion by the urinary system was not included. Since this model was a simplified lumped parameter model and did not contain a microcirculation compartment, this was a necessary assumption. Another limitation of this model was the lack of consideration of additional hormonal interactions within the cardiovascular system. These include atrial natriuretic peptide, which provides negative feedback to the renovascular system when stretch receptors on the atria detect increased stretch, and endothelin. Again, this model did not contain atrial compartments, so this was a necessary assumption. Also, the negative feedback that exists within the renin-angiotensin-aldosterone system was implemented in the system of ODEs. However, this model was a simplified version of blood volume control, focused solely on the kidneys, so great room for improved accuracy exists.

4.3 Optimization Results

The optimization methods used in this thesis were not comprehensive, but did reduce the total solving time by over 80%. This was achieved using a combination of different methods that did not affect the end result significantly, but did reduce the amount of time to get to the end result significantly.

Chapter 5: Concluding Remarks

This thesis introduced a novel approach to integrating different arterial pressure regulating time scales. While it is most common to take a unilateral approach and investigate phenomena without separation of time scales, the modularization and integration of multiple time scales allows for greater breadth of scientific investigation. In this thesis, the baroreflex was the primary player on the acute time scale, and the renin-angiotensin-aldosterone system was the key player of longer-term arterial regulation. These models were validated individually by demonstrating phenomenological similarity to previous experimental studies. An additional benefit of this model was that it was coupled to a closed-loop model of the circulation, which is fairly crucial in modeling the cardiovascular system.

In further studies, greater detail could be added to the time scales developed in this model, and more importantly, additional time scales could be integrated. This thesis began to investigate the effects of aortic stenosis on the heart, using a time-varying elastance model, but it is the recommendation of this author that longer-term growth and remodeling are coupled with the shorter time scales modeled here. The implementation of this model was optimized to aid in integrating the results with a finite element model in the future.

Since pathophysiological conditions can be challenging to study *in vivo*, computational models can be valuable tools for accessible study. However, computational models of biological systems are necessarily reductionist and never completely representative. It is the view of this author that with the advancement of scientific and technological capabilities in research, computational models will become increasingly accurate, and thus, increasingly useful.

REFERENCES

[1] Averina VA, Othmer HG, Fink GD, Osborn, JW. A new conceptual paradigm for the haemodynamics of salt-sensitive hypertension: A mathematical modeling approach. *J Physiol*. 2012, 590(Pt 23):5975-5992.

[2] Baumgartner H, Hung J, Bermejo J, Chambers JB, Evangelista A, Griffin BP, Lung B, Otto CM, Pellikka PA, Quinones M, American Society of Echocardiography, European Association of Echocardiography. Echocardiographic assessment of valve stenosis. EAE/ASE recommendations for clinical practice. *J Am Soc Echocardiogr*. 2009;22(1):1-23.

[3] Beard DA, Pettersen KH, Carlson, BE, Omholt, SW, Bugenhagen, SM. A computational analysis of the long-term regulation of arterial pressure. *F1000 Res.* 2013;2:208.

[4] Bergel DH, Anand IS, Brooks DE, MacDermott AJ, Peveler RC, Robinson JL, Sleight P. “Carotid sinus wall mechanics and baroreceptor function in the dog.” Arterial Baroreceptors and Hypertension. *Oxford Medical Publications.* 1980:1-5.

[5] Bitzblitz. “Pressure vs Volume loop for the heart”. 2010. CC BY 3.0. https://commons.wikimedia.org/wiki/File:Cardiac_Pressure_Volume_Loop.jpg.

[6] Chirinos JA. Ventricular-Arterial Coupling: Invasive and Non-Invasive Assessment. *Artery Res.* 2013;7(1).

[7] Coleridge HM, Coleridge JCG, Kaufman MP, Dangel A. Operational sensitivity and acute resetting of aortic baroreceptors in dogs. *Circ Res.* 1981;48:676-684.

[8] Coleridge HM, Coleridge JC, Poore ER, Roberts AM, Shultz HD. Aortic wall properties and baroreceptor behaviour at normal arterial pressure and in acute hypertensive resetting in dogs. *J Physiol.* 1984;350:309-326.

[9] Cowley, AW Jr. Long-term control of arterial blood pressure. *Physiol Rev.* 1992;72(1):231-300.

[10] Edwards Life Sciences. Normal Hemodynamic Parameters and Laboratory Values Irvine, CA. 2009.

[11] Faggiano P, Frattini S, Zilloli V, Rossi A, Nistri S, Dini FL, Lorusso R, Tomasi C, Cas LD. Prevalence of comorbidities and associated cardiac diseases in patients with valve aortic stenosis. Potential implications for the decision-making process. *Int J Cardiol.* 2012;159(2):94-99.

[12] Ghasemalizadeh O, Mirazee MR, Firoozabadi B, Hassani K. Exact Modeling of Cardiovascular System Using Lumped Method. *BIOCOMP.* 2008. 408-417.

[13] Guyton, A. "The Renal Function Curve--The Key to Understanding the Pathogenesis of Hypertension." Editorial. *Hypertension*, July 1, 1987.

[14] Guyton AC, Coleman TG, Granger HJ. Circulation: Overall regulation. *Annu Rev Physiol*. 1972;34:13-46.

[15] Kahn SL, Angle JF. Adrenal Vein Sampling. *Techniques in Vascular and Interventional Radiology.* 2010;13:110-125.

[16] Krieger EM. Mechanisms of baroreceptor resetting in hypertension. *Drugs.* 1988;35(Suppl 6):98-103.

[17] Kerchkoffs RCP, Omens JH, McCulloch AD. A single strain-based growth law predicts concentric and eccentric cardiac growth during pressure and volume overload. *Mech Res Commun.* 2012;42:40-50.

[18] Kopp UC. “Neuroanatomy”. Neural Control of Renal Function. *Morgan & Claypool Life Sciences.* 2011. ww.ncbi.nlm.nih.gov/books/NBK57242/.

[19] Lohmier TE, Irwin ED, Rossing MA, Serdar DJ, Kieval RS. Prolonged activation of the baroreflex produces sustained hypotension. *Hypertension.* 2004;43(2):306-311.

[20] Lu K, Clark W Jr, Ghorbel FH, Ware DL, Bidani A. A human cardiopulmonary system model applied to the analysis of the Valsalva maneuver. *Am J Physiol Heart Circ Physiol.* 2001;281:2661-2679.

[21] MATLAB and Statistics Toolbox Release 2014b, The MathWorks, Inc., Natick, Massachusetts, United States.

[22] Mulvany MJ. Vascular remodeling of resistance vessels: can we define this? *Cardiovas Res.* 1999;41:9-1310.

[23] Nakata S, Sugawara M, Hayashi H, Koyanagi H. Measurement of severity of aortic stenosis experimentally produced in dogs without inserting a catheter into the left ventricle. *Am J Cardiol.* 1985;55(8):1097-1101.

[24] Normal Hemodynamic Parameters. *LiDCO*. 2017. www.lidco.com/education/normal-hemodynamic-parameters/.

[25] O’Brien KD. Pathogenesis of Calcific Aortic Valve Disease: a disease process comes of age (and a good deal more). *Arterioscler Thromb Vasc Biol.* 2006;26(8):1721-1728.

[26] Omidvar O, Elliott DL. “Baroreceptor Reflex”. Neural Systems for Control. *Elsevier.*

1997;111-112.

[27] Ottosen JT. Modelling the dynamical baroreflex-feedback control. *Mathematical and Computer Modelling.* 2000;31(4-5):167-173.

[28] Pappano, AJ, Wier, WG, Levy, MN. Cardiovascular physiology. 9th ed. Philadelphia, PA: Elsevier/Mosby. 2013.

[29] Problem: Aortic Valve Stenosis. *American Heart Association*. 2013. www.heart.org/HEARTORG/Conditions/More/HeartValveProblemsandDisease/Problem-Aortic-Valve-Stenosis_UCM_450437_Article.jsp#.Wadgu8fiPw9.

[30] Rodriguez EK, Hoger A, McCulloch AD. Stress-dependent finite growth in soft elastic tissues. *J Biomech*. 1994;4:455-467.

[31] Santamore, WP, Burkhoff, D. Hemodynamic consequences of ventricular interaction as assessed by model analysis. *Am J Physiol.* 1991; 260(1 Pt 2):H146-157.

[32] Seagard JL, van Brederode JF, Dean C, Hopp FA, Gallenberg LA, Kampine JP. *Circ Res.* 1990;66(6):1499-1509.

[33] Sunagawa K, Maughan WL, Sagawa K. Optimal arterial resistance for the maximum stroke work in isolated canine left ventricle. *Circ Res.* 1985;56(4):586-595.

[34] Sunagawa K, Kawada T, Nakahara T. Dynamic nonlinear vago-sympathetic interaction regulating heart rate. *Heart Vessels.* 1998;13:157-174.

[35] Walley KR. Left ventricular function: time-varying elastance and left ventricular aortic coupling. *Critical Care.* 2016;20:270.

[36] Westerhof N, Bosman F, DeVies CJ, Noordergraaf A. Analog studies of the human systemic arterial tree. *J Biomech.* 1969;2:121-143.

[37] Westerhof N, Stergiopulos N, Nobel MIM. “Arterial Windkessel”. Snapshots of Hemodynamics: An Aid for Clinical Research and Graduate Education. *Springer Science + Business Media, Inc.* 2005. Print.

[38] Zahedmanesh H, Lally C. A multiscale mechanobiological modeling framework using agent-based models and finite element analysis: application to vascular tissue engineering. *Biomech Model Mechanobiol.* 2012;11:363-377.